Fermiology and Fulde-Ferrell-Larkin-Ovchinnikov Phase Formation

A. B. Kyker and W. E. Pickett
Department of Physics, University of California, Davis, California 95616, USA

F. Gygi
Center for Applied Scientific Computing, Lawrence Livermore National Laboratory, Livermore, California 94551, USA
(Received 12 January 2005; published 30 June 2005)

The Bogoliubov–de Gennes equations for singlet superconductivity in an exchange field are analyzed with real materials having complex Fermi surfaces in mind. The resulting gap equation is reformulated in terms of a velocity spectrum on the Fermi surface in which the surface geometry is built in. The resulting analysis can readily be used for arbitrary dispersion relations. Fulde-Ferrell-Larkin-Ovchinnikov (FFLO) phases are studied in the temperature-field plane, with results providing a physically clear interpretation of why certain directions of pair momentum $\vec{q}$ are energetically favored. We present clarifying results for models (the two-dimensional square Fermi surface, one-, two-, and three-dimensional isotropic surfaces) and provide an application to the weak ferromagnetic $ZrZn_2$ showing it is not a favorable case for an FFLO phase.

DOI: 10.1103/PhysRevB.71.224517 PACS number(s): 74.10.+v, 74.20.Rp, 71.18.+y

I. INTRODUCTION

Almost half a century ago Ginzburg addressed the question of possible superconductivity in ferromagnetic material[1] and studied the problems posed by orbital supercurrents within a material with intrinsic magnetic flux. About a decade later and armed with BCS theory,[2] Fulde and Ferrell[3] (FF) and separately Larkin and Ovchinnikov[4] (LO) addressed the separate question as to how a BCS superconductor copes with an intrinsic spin splitting, which breaks the degeneracy of spin-up and spin-down Fermi surfaces. Both FF and LO concluded that (neglecting orbital current effects) there is a superconducting phase (the "FFLO phase") above the usual upper critical field H_{c2} where superconductivity persists based on $\vec{q} \neq 0$ (nonzero momentum) pairs and the order parameter becomes inhomogeneous.

Since that time, there has been a considerable number of papers exploring the competition between, and possible coexistence of, the superconducting and magnetic long-range-order parameters.[5] Full treatment requires consideration of both orbital and spin effects, and for the most part theories have tended to suppose that one is dominant in a particular system and to concentrate on that one. Thus investigations have focused either on the orbital effects such as spontaneous vortex phases or on the exposition of the FFLO phase without complications from vortex behavior. Much has been accomplished with this approach, although little in a material-specific way that would allow theories to be carefully tested. With regard to the FFLO phase, the move has been in the opposite direction: make the system fit the idealizations of the theorists.

Two-dimensional (2D) layered organic crystals provide the primary playground. With negligible carrier hopping between layers, the magnetic field can be oriented nearly in-plane and the competition between spin and orbital pair breaking first studied theoretically by Bulaevskii[6] can be probed. If the field lies precisely within the layer, orbital pair breaking vanishes, leaving only a small exchange splitting ($\pm \mu_B B$) to inhibit superconductivity. This setup has led to strong evidence that a distinct high-field, low-temperature phase in κ-$(BEDT\text{-}TTF)_2Cu(NCS)_2$ is an excellent candidate for an FFLO phase.[7,8] The observed new phase seems consistent with theoretical expectations[9] and is suggested to arise due to a favorable Fermi surface shape.[7,8]

A less prosaic candidate, still within the quasi-two-dimensional realm, is λ-$(BETS)_2FeCl_4$, which contains the conducting layers of BETS molecules and layers of Fe^{3+} magnetic ions. At ambient pressure it undergoes a transition to an antiferromagnetic insulating phase below 10 K. Upon application of a field, it undergoes an insulator-to-metal transition at 11 T and then becomes superconducting above 16–17 T, with T_c increasing with field.[10,11] The field-induced superconductivity is thought to be due to the Jaccarino-Peter mechanism in which the applied field counteracts the internal exchange field due to the magnetic ions, enabling singlet pairing. At the edges of this field-induced superconducting phase, FFLO phases are expected to arise.[12] Experimental determination of the Fermi surface[13] has become a central part of the understanding of this system.

An FFLO phase has been suggested to account for a second superconducting phase deep within ($H < H_{c2}$) the main superconducting phase in $CeCoIn_5$.[14] This compound is a favorable case for an FFLO phase because it is extremely pure and due to its large Maki parameter (which indicates that orbital pair breaking is a minor effect). The transition between the suggested FFLO phase and the normal state is first order. It has also been found that the phase boundaries depend strongly on the direction of the applied field.[15] Observation of a possible FFLO phase has also been argued for UBe_{13},[16] based on a strong upturn in the upper critical field at low temperature.

Underlying the criteria for a specific superconducting phase is not only the coupling strength and character (anisotropy, for example), but also the characteristics of the Fermi surface where superconductivity "lives." It is vaguely expected, of course, that FFLO pairing is favored by "nesting" in some sense of the exchange-split Fermi surfaces. Specifi-

cally, however, little has been established quantitatively about the importance of the shape of the FS and the value and anisotropy of the Fermi velocity of the quasiparticles. These aspects can be very important for superconducting properties—for example, the symmetry of the vortex lattice can change depending on the degree of anisotropy of the Fermi velocity around the FS,[17] and the quasiparticle spectrum within a vortex is sensitive to the Fermi surface topology.[18]

FFLO phases are traditionally studied in the context of exchange splitting due to applied fields, but the same situations arise for superconductivity in weak ferromagnets (which was what FF and LO had in mind). The recent identification of several examples of superconductivity coexisting with weak ferromagnetism ($RuSr_2GdCu_2O_8$, UGe_2, URhGe, $ZrZn_2$) and in close proximity to the magnetic quantum critical point (QCP) broadens the interest in the effects of exchange splitting on pairing and superconducting phenomenology. Certainly near the QCP where the exchange splitting goes to zero, the action depends strongly on the fermiology, and Sandeman *et al.* have modeled the metamagnetic behavior of UGe_2 in terms of changing Fermi surface topology.[19] The spectrum of critical fluctuations near the QCP is also sensitive to the Fermiology, specifically the magnitude and anisotropy of the Fermi velocity.[20] In $ZrZn_2$ additional phases (differing at least in magnetic properties) have recently been observed[21] that alter the picture from what was presented originally.[22,23]

In this paper we aim to extend our understanding of materials characteristics that make an FFLO phase favorable and, at the same time, develop numerical techniques that allow the formalism to be applied to real materials with complicated Fermi surfaces, which in certain cases may favor formation of FFLO phase. At this stage we neglect effects of orbital currents, as has typically been done previously.

II. FORMALISM

A. Hamiltonian in an exchange field

The BCS (Bardeen-Cooper-Schrieffer) reduced Hamiltonian with exchange splitting $\pm\mu_B B$, in units in which $\mu_B = 1$, is

$$H = \sum_{\vec{k}} \epsilon_{\vec{k}}(n_{\vec{k}\uparrow} + n_{-\vec{k}\downarrow}) - B\sum_{\vec{k}} (n_{\vec{k}\uparrow} - n_{-\vec{k}\downarrow}) - g\sum_{\vec{k}\vec{k}'} c^{\dagger}_{\vec{k}'\uparrow} c^{\dagger}_{-\vec{k}'\downarrow} c_{-\vec{k}\downarrow} c_{\vec{k}\uparrow}. \tag{1}$$

Here $c^{\dagger}_{\vec{k}\sigma}(c_{\vec{k}\sigma})$ is the creation (destruction) operator for single-electron states, $n_{\vec{k}\sigma} \equiv c^{\dagger}_{\vec{k}\sigma} c_{\vec{k}\sigma}$, and the single-particle dispersion is referenced to the Fermi energy $\epsilon_F = 0$. The attractive pairing strength g is positive for single-particle energies $|\epsilon_{\vec{k}}|$ within a cutoff energy ϵ_c and zero otherwise. Use is made of the symmetry $\epsilon_{-\vec{k}} = \epsilon_{\vec{k}}$ to write the first two terms in an unconventional manner (involving $n_{-\vec{k}\downarrow}$ rather than $n_{\vec{k}\downarrow}$).

To accommodate the formalism to pairing of pairs with momentum of $\vec{q}$, the interaction term of the Hamiltonian is rewritten for pairing of states $(\vec{k}+\vec{q}/2)\uparrow$ with $(-\vec{k}+\vec{q}/2)\downarrow$,

$$H = \sum_{\vec{k}} \epsilon_{\vec{k}}(n_{\vec{k}\uparrow} + n_{-\vec{k}\downarrow}) - B\sum_{\vec{k}} (n_{\vec{k}\uparrow} - n_{-\vec{k}\downarrow}) - g\sum_{\vec{k}\vec{k}'} c^{\dagger}_{\vec{k}'+\vec{q}/2,\uparrow} c^{\dagger}_{-\vec{k}'+\vec{q}/2,\downarrow} c_{-\vec{k}+\vec{q}/2,\downarrow} c_{\vec{k}+\vec{q}/2,\uparrow}. \tag{2}$$

The $\vec{k}+\vec{q}/2,\uparrow$ and $-\vec{k}+\vec{q}/2,\downarrow$ indices appearing in the pairing potential can be simplified in preparation for the Bogoliubov–de Gennes (BdG) transformation

$$\tilde{c}^{\dagger}_{\vec{k}\sigma} \equiv c^{\dagger}_{\vec{k}+\vec{q}/2,\sigma}, \quad \tilde{c}^{\dagger}_{-\vec{k}\sigma} \equiv c^{\dagger}_{-\vec{k}+\vec{q}/2,\sigma}, \tag{3}$$

$$\tilde{n}_{\vec{k}\sigma} \equiv \tilde{c}^{\dagger}_{\vec{k},\sigma} \tilde{c}_{\vec{k},\sigma}. \tag{4}$$

A further simplification is made by making a small-$\vec{q}$ approximation:

$$\epsilon_{\vec{k}+\vec{q}/2} \approx \epsilon_{\vec{k}} + \frac{\vec{q}}{2}\cdot\vec{v}_{\vec{k}}, \quad \vec{v}_{\vec{k}} \equiv \vec{\nabla}\epsilon_{\vec{k}}. \tag{5}$$

The Fermi surface that defines $\vec{v}_{\vec{k}}$ at $\vec{k} = \vec{k}_F$ is the non-spin-polarized normal-state Fermi surface. With the linear approximation, the normal-state Fermi surface marks the superconducting state's chemical potential.

After collecting operators with common $\vec{k}$, the Hamiltonian for nonzero momentum becomes

$$H = \sum_{\vec{k}} \epsilon_{\vec{k}}(\tilde{n}_{\vec{k}\uparrow} + \tilde{n}_{-\vec{k}\downarrow}) + \sum_{\vec{k}} \left(\frac{\vec{q}}{2}\cdot\vec{v}_{\vec{k}_F} - B\right)(\tilde{n}_{\vec{k}\uparrow} - \tilde{n}_{-\vec{k}\downarrow}) - g\sum_{\vec{k}\vec{k}'} \tilde{c}^{\dagger}_{\vec{k}'\uparrow}\tilde{c}^{\dagger}_{-\vec{k}'\downarrow}\tilde{c}_{-\vec{k}\downarrow}\tilde{c}_{\vec{k}\uparrow} = \sum_{\vec{k}\sigma} \xi_{\vec{k}\sigma}\tilde{n}_{\vec{k}\sigma} - g\sum_{\vec{k}\vec{k}'} \tilde{c}^{\dagger}_{\vec{k}'\uparrow}\tilde{c}^{\dagger}_{-\vec{k}'\downarrow}\tilde{c}_{-\vec{k}\downarrow}\tilde{c}_{\vec{k}\uparrow}, \tag{6}$$

where the spin-dependent dispersion is given by

$$\xi_{s_\sigma\vec{k}\sigma} = \epsilon_{\vec{k}} + s_\sigma w_{\vec{k}}, \quad w_k \equiv \frac{\vec{q}}{2}\cdot\vec{v}_{\vec{k}_F} - B, \quad s_\uparrow \equiv 1, \quad s_\downarrow \equiv -1. \tag{7}$$

In this form several new features can be understood. First, because of the convention of associating $\vec{k}$ with up spin and $-\vec{k}$ with down spin and assuming inversion symmetry of the Fermi surface, the pair momentum $\vec{q} \neq 0$ acts so as to add another *effective* Zeeman splitting term to the Hamiltonian. Second, the new Zeeman splitting term is a peculiar one that varies over the Fermi surface. A central feature in the physics and understanding of the resulting phenomena is that for one-half of the Fermi surface these splittings (from B and from $\vec{q}$) tend to cancel, which enables FFLO superconducting states to arise.

B. Bogoliubov-Valatin transformation

The mean-field approximation for the superconducting state consists of presuming the appearance of an order parameter

$$b_k = \langle \tilde{c}_{-k\downarrow}\tilde{c}_{k\uparrow}\rangle, \tag{8}$$

introducing the tautology

$$\tilde{c}_{-k\downarrow}\tilde{c}_{k\uparrow} = b_k + (\tilde{c}_{-k\downarrow}\tilde{c}_{k\uparrow} - b_k), \tag{9}$$

and neglecting the product of the fluctuations (terms in parentheses) in the interaction term. In the case we consider b_k gives the amplitude for finding a pair with momentum $\vec{q}$ and zero spin in the superconducting state. The "energy gap" (see below for clarification) is given by

$$\Delta = g\sum_k b_k, \tag{10}$$

from which it is seen that the assumption of an isotropic coupling matrix elements g leads to an isotropic gap. The Hamiltonian becomes

$$H = \sum_{\vec{k}\sigma} \xi_{k\sigma}\tilde{n}_{\vec{k}\sigma} - \sum_{\vec{k}} [\Delta\tilde{c}^{\dagger}_{\vec{k}'\uparrow}\tilde{c}^{\dagger}_{-\vec{k}'\downarrow} + \text{H . c.}]. \tag{11}$$

The resulting mean-field Hamiltonian is diagonalized by a Bogoliubov–Valatin (BV) transformation, leading to the Bogoliubov-de Gennes equations. In general, the BV transformation leads to quasiparticles that are superpositions of electrons and holes with both up and down spin. The Hamiltonian matrix which defines the quasiparticle eigenamplitudes and eigenenergies is

$$\begin{pmatrix} \epsilon_{\vec{k}} + w_k & 0 & 0 & \Delta \\ 0 & \epsilon_{\vec{k}} - w_k & -\Delta & 0 \\ 0 & -\Delta^* & -\epsilon_{-\vec{k}} - w_k & 0 \\ \Delta^* & 0 & 0 & -\epsilon_{\vec{k}} + w_k \end{pmatrix} \times \begin{pmatrix} C_{\tau,\vec{k}\uparrow} \\ C_{\tau,-\vec{k}\downarrow} \\ D_{\tau,\vec{k}\uparrow} \\ D_{\tau,-\vec{k}\downarrow} \end{pmatrix} = E_{\tau,\vec{k}} \begin{pmatrix} C_{\tau,\vec{k}\uparrow} \\ C_{\tau,-\vec{k}\downarrow} \\ D_{\tau,\vec{k}\uparrow} \\ D_{\tau,-\vec{k}\downarrow} \end{pmatrix}, \tag{12}$$

where τ is an index for the four possible quasiparticle states and C and D are the coefficients for the single-particle creation and destruction operators, respectively.

The expression of Powell, Annett, and Gyorffy[24] for more general types of pairing (albeit only $\vec{q}=0$) reduces to this form for singlet pairing. Diagonalizing the matrix, which reduces to a pair of 2×2 matrices, produces four branches of quasiparticles states with definite spin and eigenenergies

$$E^{\pm}_{s_\sigma \vec{k}\sigma} = s_\sigma w_{\vec{k}} \pm \sqrt{\epsilon^2_{\vec{k}} + \Delta^2} \tag{13}$$

and which obey the Fermion anticommutator relations.

In the superconducting ground state with $w_{\vec{k}}=0$, all of the negative-energy states will be occupied. The positive-energy states can then be considered quasiparticle excitations. The rest of the analysis will be in terms of these excitations. The quasiparticle operators are

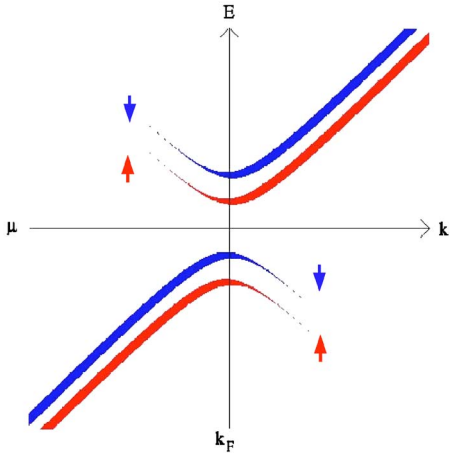

FIG. 1. (Color online) Sketch of the four branches of the quasiparticle dispersion in a magnetic superconductor. An energy gap of 2Δ opens at the Fermi surface between quasiparticles with common spin direction. The exchange splitting will reduce the opposite-spin gap, but does not directly effect the superconducting parameter Δ. The thickness of the line represents the electron character of the quasiparticles.

$$\gamma^{\dagger}_{\vec{k}\uparrow} = u_{\vec{k}}\tilde{c}^{\dagger}_{\vec{k}\uparrow} + 0 + 0 - v_{\vec{k}}\tilde{c}_{-\vec{k}\downarrow},$$

$$\gamma^{\dagger}_{-\vec{k}\downarrow} = 0 + u_{\vec{k}}\tilde{c}^{\dagger}_{-k\downarrow} + v_{\vec{k}}\tilde{c}_{k\uparrow} + 0,$$

$$\gamma_{\vec{k}\uparrow} = 0 - v_{\vec{k}}\tilde{c}^{\dagger}_{-k\downarrow} + u_{\vec{k}}\tilde{c}_{k\uparrow} + 0,$$

$$\gamma_{-\vec{k}\downarrow} = v_{\vec{k}}\tilde{c}^{\dagger}_{\vec{k}\uparrow} + 0 + 0 + u_{\vec{k}}\tilde{c}_{-\vec{k}\downarrow}, \tag{14}$$

where $u_{\vec{k}}$ and $v_{\vec{k}}$ are given by

$$\sqrt{2}u_{\vec{k}} = \sqrt{1 + \frac{\epsilon_{\vec{k}}}{\sqrt{\epsilon^2_{\vec{k}} + \Delta^2}}},$$

$$\sqrt{2}v_{\vec{k}} = \sqrt{1 - \frac{\epsilon_{\vec{k}}}{\sqrt{\epsilon^2_{\vec{k}} + \Delta^2}}}. \tag{15}$$

The BCS results are recovered when $w_k=0$ and $\vec{q}=0$. It is interesting that the quasiparticle amplitudes $u_{\vec{k}}$ and $v_{\vec{k}}$ are independent of the Zeeman splitting. This can be understood by noting that w_k in each 2×2 submatrix enters proportional to the identity matrix.

C. Gap equation

The quantity 2Δ becomes the gap between the quasiparticle eigenenergies with common spin label. The actual *opposite-spin gap* $2\Delta - 2|w_{\vec{k}}|$ does not enter the gap equation directly, and the quasiparticle energies enter only through the Fermi occupation functions. The quasiparticle bands are pictured in Fig. 1. The gap equation is given by

$$\Delta = g\sum_{\vec{k}} u_{\vec{k}} v_{\vec{k}} [1 - f(E^{+}_{\vec{k}\uparrow}) - f(E^{+}_{-\vec{k}\downarrow})]. \tag{16}$$

Since the index $\vec{k}$ now enters through the energy term $s_\sigma(\vec{q}/2)\cdot\vec{v}_{\vec{k}}$ as well as through $\epsilon_{\vec{k}}$, it is no longer possible to simply change the $\vec{k}$ summation to a one-dimensional energy integral scaled by the density of states at the Fermi surface, which is the technique typically applied when the Zeeman term is not $\vec{k}$ dependent.

Introducing the integral over the δ function $1=\int\delta(\hat{q}\cdot\vec{v}_{\vec{k}_F} - V)dV$ in addition to the usual one $1=\int\delta(\epsilon-\epsilon_k)d\epsilon$ leads to the form of the gap equation that we focus on:

$$\Delta = N_0 g \int dV N(V,\hat{q}) \int_{-\epsilon_c}^{\epsilon_c} d\epsilon \frac{\Delta}{2\sqrt{\epsilon^2+\Delta^2}} [1 - f(E^{+}_{\uparrow}) - f(E^{+}_{\downarrow})]$$
$$= \lambda \int dV N(V,\hat{q}) K\left(\Delta, T, \frac{1}{2}qV - B\right). \tag{17}$$

N_0 is the density of states evaluated at E_F and we introduce the usual coupling strength $\lambda = N_0 g, E^{(+)}_{\sigma}$ is given by Eq. (13) with $\epsilon_{\vec{k}} \to \epsilon$, and the variation in $N(E)$ within ϵ_c of the Fermi level has been neglected. This expression reduces to the BCS equation when $|\vec{q}|=0$. The dependence on exchange splitting enters only through the quasiparticle eigenenergies. In the second expression the kernel K already includes the energy integral.

The new function that has been introduced is the Fermi surface projected-velocity distribution that depends on the direction of $\vec{q}$,

$$N(V,\hat{q}) = \frac{1}{N_0}\sum_{\vec{k}} \delta(\epsilon_F - \epsilon_{\vec{k}})\delta(\hat{q}\cdot\vec{v}_{\vec{k}_F} - V)$$
$$= \frac{1}{N_0}\frac{\Omega_c}{(2\pi)^3}\oint_{fs}\frac{\delta(\hat{q}\cdot\vec{v}_{\vec{k}_F} - V)}{|\vec{v}_{\vec{k}_F}|}ds, \tag{18}$$

which is normalized as

$$\int N(V,\hat{q})dV = 1. \tag{19}$$

$N(V,\hat{q})$ will be called the *nesting density* for reasons related to FFLO phase formation. The Fermi surface geometry and the variation of the velocity get folded into $N(V,\hat{q})$, which incorporates the local density of states factor $1/|\vec{v}_{\vec{k}_F}|$. The energy integral $K\left(\Delta, T, \frac{1}{2}qV - B\right)$ remains independent of the details of the Fermi surface.

We will explore the solutions to the gap equation while varying the parameters T, B, Δ, and q for a given dispersion relation $\epsilon_{\vec{k}}$ and coupling strength λ. It will also be of interest to consider variations in the direction of the pair momentum; however, we will restrict ourselves to directions of high symmetry since these directions will provide extrema of the functions by symmetry considerations.

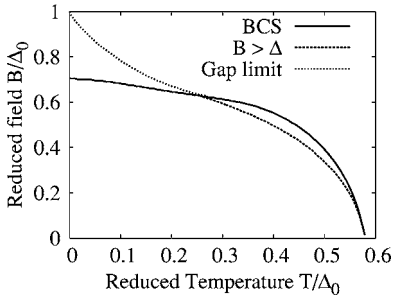

FIG. 2. The phase diagram in the T-B plane. The solid line marks the BCS to normal phase transition. The region between the "$B>\Delta$" and "BCS" lines has no opposite-spin excitation gap but superconducting pairing still exists. Solutions to the gap equation exist for B under the "Gap limit," but the free energy of the normal phase is lower than the BCS phase. The "$B>\Delta$" and "Gap limit" do not meet "BCS" at the same point.

III. COEXISTENCE OF MAGNETIZATION AND SUPERCONDUCTIVITY

A. BCS phase

We first mention the BCS phase diagram in the T-B plane. Band-crossing-induced magnetization and $\vec{q}=0$ (BCS) pairing coexist near the first-order phase boundary between $T \approx T_c/2$ and $T=T_c$. In this region where $|B|>\Delta>0$, the gap between opposite-spin quasiparticles closes, giving rise to field-induced pair breaking at the Fermi surface, while pairing occurs away from the Fermi surface. When $|B|<\Delta$, an opposite-spin gap exists over the entire Fermi surface, and spin splitting can only occur for thermally broken pairs. The general phase diagram is illustrated in Fig. 2.

B. FFLO phase

The FFLO phase takes advantage of the Zeeman energy due to magnetization that arises when $B>\Delta$, but then uses a finite pair momentum to enhance pairing. A graphical way of understanding this enhanced pairing through the quasiparticle Fermi surface is shown in Fig. 3. The closing of the opposite-spin gap shrinks the minority-spin Fermi surface while expanding the majority spin (see Fig. 4). The coupling of the pair momentum to the quasiparticle eigenenergy is then used to reopen an opposite-spin gap on part of the Fermi surface. Due to inversion symmetry of the dispersion relationship $\epsilon_{\vec{k}}$, spin splitting on the opposite side of the Fermi surface is increased. This trade-off can be energetically favorable because pairing is strongest near the Fermi surface. Nesting can be said to occur on the portions of the Fermi surface where spin splitting is eliminated by a given $\vec{q}$.

FFLO phases are favored when (1) enough of the Fermi surface can be paired (nesting is strong enough) to allow for a superconducting ($\Delta \neq 0$) solution to the gap equation and (2) the FFLO free energy is less than the BCS free energy and normal paramagnetic free energy. Using the form of the gap equation that includes the nesting density, we want to understand what features of the Fermi surface favor the FFLO state. For a given splitting and direction of $\hat{q}$, the lowest FFLO free energy occurs when pairing is maximized.

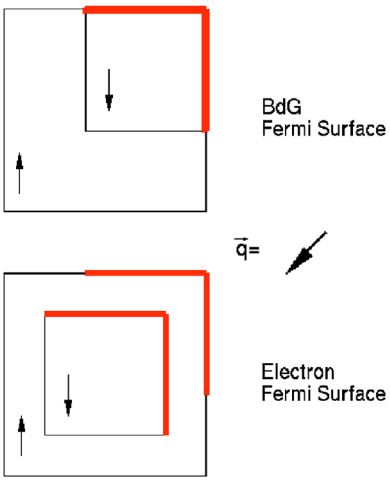

FIG. 3. (Color online) The top graph represents occupied BdG quasiparticle states in $\vec{k}$ and $-\vec{k}$ space for spin up and spin down, respectively, for 2D square Fermi surfaces. This nonstandard representation highlights how the pairing momentum nests the Fermi surfaces by canceling the magnetic induced splitting—greatly exaggerated here—to enable pairing (shown as the thick line). The bottom graph shows the electron Fermi surfaces which remain unshifted by the pair momentum.

Pairing is enhanced when $\frac{1}{2}qV=(\vec{q}/2)\cdot\vec{v}_{\vec{k}_F}$ is chosen to cancel the magnetic splitting on some part of the Fermi surface. The value of q selects the range of V where $|\frac{1}{2}qV-B|<\Delta$ (e.g., where nesting occurs).

The effective width of nesting in V space can be found by noting when the quasiparticle eigenenergies are greater than zero at the Fermi surface. Rewriting the inequality as $|\frac{1}{2}q(V_0+\delta V)-B|<\Delta$, we find

$$\delta V \approx \frac{2\Delta}{q} \approx \left|\frac{V_0\Delta}{B}\right|, \tag{20}$$

where V_0 solves the equation $|\frac{1}{2}qV_0-B|=0$. In general, V_0 will be optimal near a peak in the nesting density and as large as possible to maximize δV.

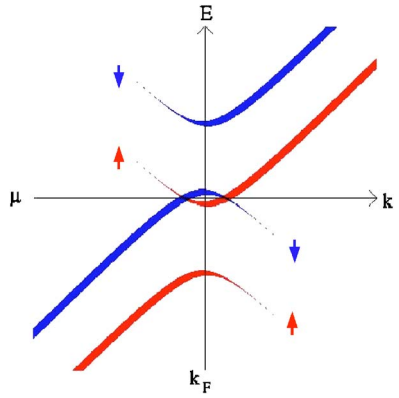

FIG. 4. (Color online) BdG quasiparticle excitations occur when the combination of the magnetic exchange splitting and pair-momentum-induced splitting are greater than Δ. The closing of the opposite-spin gap corresponds to the separation of the quasiparticle Fermi surfaces in Fig. 3 and results in the breaking of pairs on the Fermi surface.

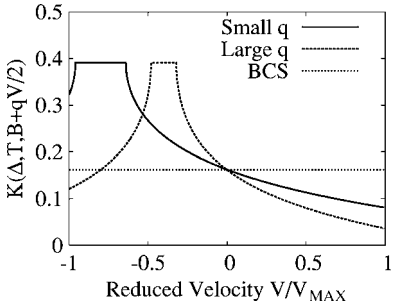

FIG. 5. Graph of the energy integral kernel $[K(\Delta,T,\frac{1}{2}qV-B)]$ from the gap equation (17) as a function of V for two values of q, fixed Δ, and $T=0$. The plateau occurs where the magnitude of the exchange splitting energy is less than Δ since this is where both quasiparticle eigenenergies are positive at the Fermi surface. The sharp drop at the edge of the plateau reflects the breaking of pairs away from the optimal nesting region.

Figure 5 illustrates the behavior of $K(\Delta,T,\frac{1}{2}qV-B)$ for two possible choices of q which solve the equation $|\frac{1}{2}qV_0-B|=0$ at different values of V_0 and fixed $\Delta<B$.

IV. APPLICATIONS OF NESTING DENSITY TO FFLO CALCULATIONS

For the calculations, we normalize $\Delta(B=0,T=0)=\Delta_0=1$ to specify the energy scale for the problem. The energy cutoff for the gap equation is a parameter that is set to $\epsilon_c=50\Delta_0$. In a real material the energy cutoff would be determined by the pairing boson (phonon, spin fluctuation, etc.). With the above parameter set, the coupling strength λ now becomes a function of ϵ_c and Δ_0, given by

$$\frac{1}{\lambda}=\sinh^{-1}\left(\frac{\epsilon_c}{\Delta_0}\right). \tag{21}$$

In the weak-coupling regime ($\lambda\equiv N_o g\ll 1$) this reduces to the well-known BCS relation $\Delta_0=2\epsilon_c e^{-1/\lambda}$. This coupling strength is $\lambda\approx 0.2$ which is well within the weak-coupling regime for which the equations were derived.

The free-energy competition between BCS and FFLO is an important factor in determining whether an FFLO state will exist. Even in the best case, at $T=0$ the free-energy-driven transition from BCS to FFLO occurs very near the

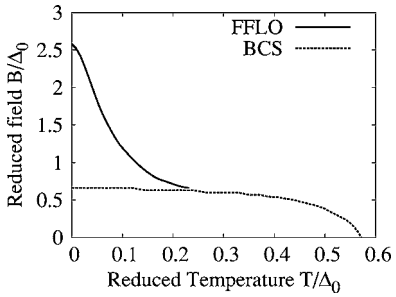

FIG. 6. The phase diagram of a 1D system. The presence of a δ function in the nesting density guarantees that half the density of states at the Fermi surface can always be paired.

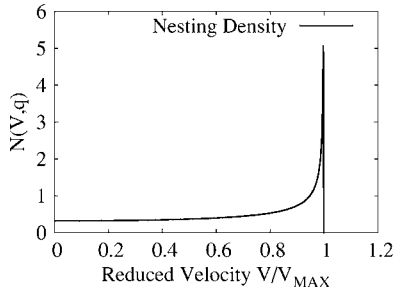

FIG. 7. The nesting density of a 2D circular Fermi surface for positive V showing peak at $V=|v_F|$. The optimal FFLO solution will choose a value for q such that this peak has enhanced pairing. The nesting density is symmetric around $V=0$ due to inversion symmetry of the Fermi surface.

BCS critical field which is proportional to the density of states at the Fermi surface. The FFLO critical field calculation is more complex. A higher proportion of FFLO pairs occur in electron states away from the Fermi surface and on average pay a higher kinetic energy cost. However, to first order the FFLO critical field is determined by the fraction of nesting density where pairing occurs at the Fermi surface. If the FFLO critical field is less than the BCS critical field for a material, no FFLO states will exist.

A. 1D Fermi surface

The simplest case is the 1D Fermi surface. The nesting density consists of δ functions at $\pm v_F$. The resulting phase diagram is given in Fig. 6. At $T=0$, solutions to the gap equation extend to arbitrarily large B with a correspondingly large $q=2B/v_F$. Free-energy constraints, however, limit the FFLO phase to finite B.

B. 2D Fermi surface

The nesting density of states for 2D Fermi surfaces will tend to have van Hove–like singularities that produce strong peaks in $N(V,q)$ that go as $1/\sqrt{|V_{peak}-V|}$. These peaks arise whenever $V=\hat{q}\cdot\vec{v}_F$ is at a local extremum. A simple example is the circular Fermi surface. The projected velocity is $V=|v_F|\cos(\phi)$ where ϕ is the angle between $\vec{v}_F$ and $\hat{q}$. Figure 7 is the nesting density for positive V and shows the peak caused by the extrema that occurs when $\hat{q}$ is normal to the Fermi surface. Figure 8 shows the phase diagram for the circular Fermi surface. From Eq. (20), we know that as B is

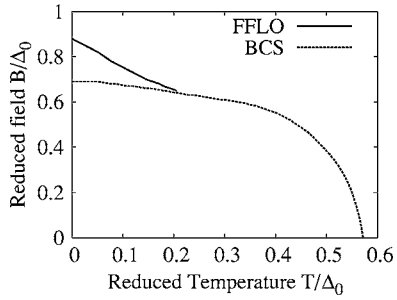

FIG. 8. The phase diagram of a 2D circular Fermi surface.

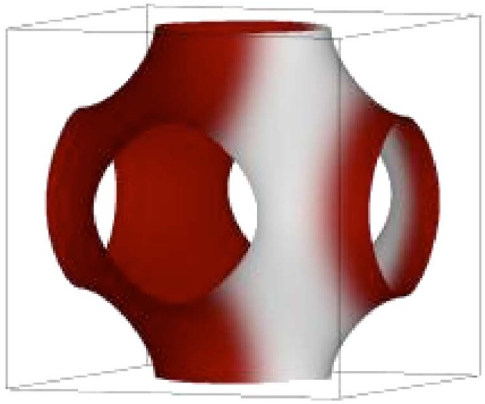

FIG. 9. (Color online) Tight-binding Fermi surface at half filling. The highlighted region corresponds to the part of the Fermi surface where enhanced pairing occurs for $T=0$, $B\approx 0.9$, and $\hat{q}=100$.

raised, the width of pairing (δV) will go down. This happens directly through the increase of q necessary to maintain V_0 near the peak and indirectly through the reduction in Δ caused by the decrease in pairing. This reduction in pairing as B is raised causes the FFLO phase to be quenched much earlier than the 1D case.

C. 3D Fermi surface

While the nesting density for 3D material may have peaks, in most cases these peaks will not be caused by van Hove singularities. This can be understood by noting that any extrema in the projected velocity will usually occur at isolated points on the Fermi surface. For example, on the spherical Fermi surface, the extrema of V occur at the two points where $\hat{q}$ is normal to the Fermi surface. The nesting density for a spherical Fermi surface is constant between $\pm|v_F|$, and consequently our calculations have shown a very small FFLO region in the phase diagram.

A 3D example with a strong peak in the nesting density at V_{max} is simple cubic nearest-neighbor tight-binding model at half filling. With q taken in the 100 direction, the projected velocity as a function of the position on the Fermi surface is given by

$$V = V_{max}\sin(k_x). \tag{22}$$

V has extrema at $k_x=\pm\pi/2$ which occurs along a curve defined by $\cos(k_y)+\cos(k_z)=0$. Since extrema occur along a curve rather than a point, $N(V,\hat{q})$ will have integrable divergences that go as $(|V_{peak}-V|)^{-1/2}$. Figure 9 is the tight-binding Fermi surface with the enhanced pairing region highlighted. The nesting density is similar to that shown in Fig. 7 with slightly more weight in the peak. Because of the increased weight, the resulting phase diagram seen in Fig. 10 shows an increased FFLO region relative to the circular Fermi surface case. Any deviation from the 100 direction will cause the extrema in V to occur at isolated points.

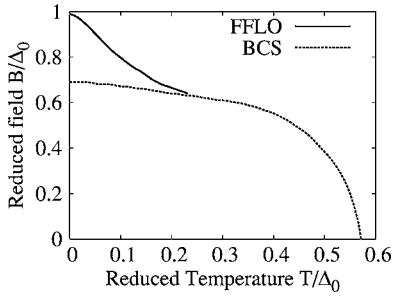

FIG. 10. Tight-binding phase diagram shows a larger FFLO region than the circular phase diagram 8. This reflects the fact that the nesting density for the tight-binding case has more weight near V_{max}.

V. $ZrZn_2$

We chose to apply our methods to $ZrZn_2$ since it has a relatively simple cubic structure, and as a weak ferromagnet with superconductivity reported at 290 mK,[23] it is a possible candidate to show an FFLO phase. A non-spin-polarized electronic structure calculation was performed using the FPLO (Ref. 25) electronic structure code. The resulting four conduction bands and Fermi surfaces have been presented by Singh and Mazin.[26] The nesting density for the four bands that cross the Fermi surface were combined into a single $N(V,\hat{q})$ function. This represents the case of equal pairing on all bands, consistent with our constant Δ model. The most favorable direction of $\hat{q}$ was found to be in the 111 direction after considering nesting properties for the three high-symmetry directions. The nesting density is shown in Fig. 11. Most of the contribution to the density of states comes from the "cubic"-shaped Fermi surface shown in Fig. 12 that Singh and Mazin call band 3. The large peak in the nesting density does not come from the nesting of the faces of the cube as one might expect but instead comes from the nesting of the grooves along the edges of the cube. The Fermi velocity on the faces is at least twice as large as the Fermi velocity along the grooves. The high value of the Fermi velocity on the faces reduces the contribution to the density of states, and variations of the Fermi velocity spread out the contribution to the nesting density over a range of V values.

The position of the largest peak gives the optimum value V_0 which in conjunction with B can be used to calculate the pair momentum $q=2B/V_0$. While this is a substantial peak, it

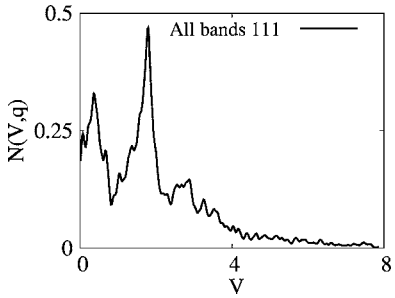

FIG. 11. $ZrZn_2$ nesting density. The units of V are 10^7 cm/sec. A small nonzero density extends to higher values of V. The noise is a function of both the finite sampling of the Fermi surface and the complexity of the electronic structure.

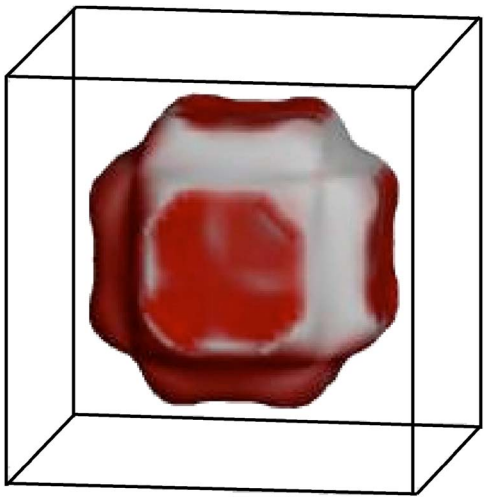

FIG. 12. (Color online) Fermi surface for the cube shape that is responsible for the peak in the nesting density 11. The highlighted region corresponds to the part of the Fermi surface where enhanced pairing occurs for $T=0, B\approx 0.6$, and $\hat{q}=111$. It is interesting that the pairing is not favored on the relative flat faces of the cube.

occurs at a low value of $|V|$ which will require a high pair momentum. As was illustrated in Fig. 5, high pair momentum reduces the amount of total density available for pairing. While FFLO solutions exist for the gap equation, at no point was the free energy of these solutions below both the free energy for the BCS phase and the normal phase.

By allowing a nonuniform Δ, it may be possible for FFLO solutions to exist in a small region above the BCS phase; however, other considerations make this unlikely. In the Hamiltonian we have assumed, the Zeeman splitting term B for ferromagnets includes the applied field as well as the ferromagnetic exchange energy. The average exchange splitting B for $ZrZn_2$ can be calculated as

$$B = \frac{M}{2N_0} \approx 30 \text{ meV} \tag{23}$$

(where $M\approx 0.15\mu_B$ and and we have used the Singh-Mazin value $N_0=2.43$ states/eV-spin-unit cell). Since the Curie temperature is greater than the observed superconducting temperature, we are not able to determine $\Delta_0=\Delta(T=0, B=0)$ for $ZrZn_2$. We can, however, place a lower bound on Δ_0 for singlet pairing by noting that, even allowing for FFLO solutions, the maximum B will be on the order of $\Delta_0/\sqrt{2}$. The resulting Δ_0 is three orders of magnitude too large as it would correspond to a $T_c\approx 2\Delta_0/3.52k_B=280$ K. From this we conclude that singlet pairing of either BCS or FFLO states is highly unlikely in bulk $ZrZn_2$.

Recent evidence has been presented that the superconductivity observed in samples of $ZrZn_2$ is a surface phenomenon,[21] consistent with the lack of any signal in the heat capacity. The superconductivity may arise from some non-$ZrZn_2$ phase in the surface region. Alternatively, it may be that the magnetic moment is strongly suppressed in the surface region, which would decrease B and tend to favor an FFLO phase. Our analysis, however, shows that the $ZrZn_2$

Fermi surface does not present a favorable platform for FFLO formation even for very weak ferromagnetism.

VI. CONCLUSION

We have presented the formalism for the specific case of the quasiparticle states and eigenenergies for non-zero momentum BdG quasiparticles in an exchange field. These quasiparticles were then used to solve the superconducting gap equation within the mean-field approximation. The spin-polarized BdG formalism was then applied to study FFLO states which have a magnetically induced spin splitting leading to pair-momentum-enhanced superconducting pairing on a subset of the Fermi surface. The *nesting density*, which is derived from the Fermi surface of the material being studied, was separated out and calculated to facilitate solving the gap equation and calculating free energies and other observables. In addition to providing an efficient means of performing calculations, the nesting density also proved to be a useful tool for understanding what features of a Fermi surface contribute to the formation of FFLO states.

The features of a Fermi surface which promote FFLO states are low dimensionality, specific nesting topographies (different from those that drive charge- and spin-density waves), and relatively simple Fermi surfaces with a uniform magnitude of the Fermi velocity. The benefits of low dimensionality is demonstrated by circular versus spherical Fermi surfaces. The tight-binding Fermi surface illustrates the benefits of nesting topographies. We emphasize that the nesting topography in this case is not a "flat sheet" which we intuitively associate with nesting. The fact that FFLO states are enhanced by peaks in the nesting density at high values of V is in conflict with the reduced density of states associated with high Fermi velocities. Variations in the magnitude of the Fermi velocity will tend to place larger weights at small V which are less likely to participate in FFLO pairing.

To simplify the calculations and analysis, we chose to consider only a uniform exchange splitting which could arise from uniform ferromagnetic exchange field or from an applied field. The BdG formalism does not depend on these assumptions and could be applied to more complex situations that do not make use of a constant exchange splitting and linearized Fermi surface approximation.

We have shown that $ZrZn_2$ (whose reported coexistence of superconductivity with ferromagnetism is now being questioned[22]) is not a favorable platform for FFLO phase formation. Two other superconducting ferromagnets are UGe_2 and URhGe, neither of which can be FFLO materials within our theory. Both have very strong spin-orbit coupling,[27,28] which means that each Fermi surface is a combination of up- and down-spin characters (which varies over the surfaces) and our theory deals only with the weak spin-orbit limit. In addition, the magnetic moments are much too large to make FFLO phase formation feasible. The possibility of FFLO phases in other weak ferromagnets, such as Sc_3In (Ref. 29) or doped $TiBe_2$ (Ref. 30), or the heavy-fermion material $CeCoIn_5$ (Refs. 14, 15, and 31) and the strong candidate (Refs. 7 and 8) κ-$(BEDT\text{-}TTF)_2Cu(NCS)_2$ for a field-induced FFLO phase, will be left for future study.

ACKNOWLEDGMENTS

W.E.P. acknowledges discussions with B.L. Gyorffy and the hospitality of the Kavli Institute of Theoretical Physics at the University of California Santa Barbara during the early stages of this work. A.K. was supported by the U.S. Department of Energy through Lawrence Livermore National Laboratory under Contract No. W-7405-ENG-48. W.E.P. acknowledges the support of National Science Foundation Grant No. DMR-0421810.

APPENDIX A: FREE-ENERGY CALCULATIONS

In all cases, the total energy of the system was calculated relative to the ground state of the normal metal at $T=B=0$:

$$E_g = 2\sum_{\vec{k}<\vec{k}_F} \epsilon_{\vec{k}}. \tag{A1}$$

With $\epsilon_c=50$ and $[B,T,\Delta]\sim 1$ in units where $\Delta_0 \equiv 1$, excitations outside the cutoff can be ignored. The free energy of the superconducting state when measured relative to the ground state becomes

$$\begin{aligned} E_s - E_g = \sum_{|\epsilon_{\vec{k}}|<\epsilon_c} \Bigg\{ & (\epsilon_{\vec{k}} + w_{\vec{k}})[v_{\vec{k}}^2 f(E_{\vec{k}\uparrow}^-) + u_{\vec{k}}^2 f(E_{\vec{k}\uparrow}^+)] + (\epsilon_{\vec{k}} - w_{\vec{k}}) \\ & \times [v_{\vec{k}}^2 f(E_{\vec{k}\downarrow}^-) + u_{\vec{k}}^2 f(E_{\vec{k}\downarrow}^+)] + \left(\epsilon_{\vec{k}} + \frac{q}{2}V_{\vec{k}}\right)\left[\Theta\left(\epsilon_{\vec{k}} + \frac{q}{2}V_{\vec{k}}\right) - 1\right] + \left(\epsilon_{\vec{k}} - \frac{q}{2}V_{\vec{k}}\right)\left[\Theta\left(\epsilon_{\vec{k}} - \frac{q}{2}V_{\vec{k}}\right) - 1\right]\Bigg\} \\ & - TS - \frac{\Delta^2}{g}. \end{aligned} \tag{A2}$$

The first two terms account for the kinetic energy of the electron part of the quasiparticles. The next two terms remove the kinetic energy for the ground state E_g. The last two terms are, respectively, the entropy and pairing potential energy. In doing the calculation this way, we have ignored the affect of the pairing energy $(q/2)V_{\vec{k}}$ on the energy cutoff which bounds the sum. With $\epsilon_c=50$ the impact is negligible, but for smaller cutoff energies it becomes important.

APPENDIX B: NUMERICAL METHODS

The first step in performing these calculations is to produce the nesting density of states. This is accomplished by extracting a triangulation of the Fermi surface with Fermi velocities from a dispersion relationship expressed on a grid. The nesting density of states integral is converted to a sum and stored in a discrete histogram indexed by $V=\hat{q}\cdot\vec{v}_{\vec{k}_F}$:

$$N(V,\hat{q}) = \frac{\Omega_c}{(2\pi)^3}\sum_i \frac{\text{Area}_i}{\vec{v}_{Fi}} \times \Theta\left(\frac{1}{2}V_\delta - |V - \hat{q}\cdot\vec{v}_{\vec{k}_F i}|\right), \tag{B1}$$

where V_δ is the projected velocity bin width and i goes over all triangles. The preferred direction for $\hat{q}$ can be found by looking for largest peaks at high V in the nesting density

calculated for each of the high-symmetry directions.

To determine the preferred state at a given temperature and applied field, it is necessary to calculate the free energy for each possible state. Furthermore, the possible superconducting states have Δ and q degrees of freedom. Fortunately, the constraint set by holding g constant means that we only need to search 1D isocontours in $\Delta - q$ space, which we evaluate on a discrete grid. Finding this isocontour requires that that we perform the integral in Eq. (17) many times.

Since we have already discretized $N(V,\hat{q})$, the integral over V becomes a sum. This leaves the energy integral

$$\int_{-\epsilon_c}^{\epsilon_c} \frac{1}{2\sqrt{\epsilon^2+\Delta^2}}[1-f(E_\uparrow^+)-f(E_\downarrow^+)]d\epsilon. \tag{B2}$$

This is a difficult integral to do numerically since it is highly peaked around $\epsilon=0$ and the behavior of the Fermi functions is highly temperature dependent. We chose to take advantage of the fact that we know how to do part of the integral analytically:

$$\int \frac{1}{2\sqrt{\epsilon^2+\Delta^2}}d\epsilon = \frac{1}{2}\sinh^{-1}\left(\frac{\epsilon_b}{\Delta}\right). \tag{B3}$$

This allows one to write formally

$$\int_{-\epsilon_c}^{\epsilon_c} \frac{1}{2}[1-f(E_\uparrow^+)-f(E_\downarrow^+)]d\left[\sinh^{-1}\left(\frac{\epsilon}{\Delta}\right)\right]. \tag{B4}$$

This integral was discretized in a manner that allowed dealing with variations in the Fermi functions. The numeric integral becomes

$$\sum_{\epsilon_i}[1-f(E_\uparrow^+)-f(E_\downarrow^+)] \tag{B5}$$

$$\left[\sinh^{-1}\left(\frac{\epsilon_i+\epsilon_{step}}{\Delta}\right)-\sinh^{-1}\left(\frac{\epsilon_i}{\Delta}\right)\right], \tag{B6}$$

with the variable step size

$$\epsilon_{step} \propto \left[\frac{\partial}{\partial\epsilon}[f(E_\uparrow^+)+f(E_\downarrow^+)]+\delta\right]^{-1}. \tag{B7}$$

The constant δ is needed to maintain a minimum step size. This variable-step integration is used in calculating contributions to the free energies and other observables of interest.

[1] V. L. Ginzburg, Sov. Phys. JETP **4**, 153 (1957).
[2] J. Bardeen, L. N. Cooper, and J. R. Schrieffer, Phys. Rev. 108 (1957).
[3] P. Fulde and R. A. Ferrell, Phys. Rev. **135**, A550 (1964).
[4] A. I. Larkin and Y. N. Ovchinnikov, Sov. Phys. JETP **20**, 762 (1965).
[5] R. Casalbuoni and G. Nardulli, Rev. Mod. Phys. **76**, 263 (2004).
[6] L. N. Bulaevskii, Sov. Phys. JETP **38**, 634 (1974).
[7] M. S. Nam, J. A. Symington, J. Singleton, S. J. Blundell, A. Ardavan, J. A. A. A. Perenboom, M. Kurmoo, and P. Day, J. Phys.: Condens. Matter **11**, L477 (1999); J. A. Symington, J. Singleton, M. S. Nam, A. Ardavan, M. Kurmoo, J. A. Schlueter, and P. Day, Synth. Met. **120**, 711 (2001).
[8] J. Singleton, J. A. Symington, M. S. Nam, A. Ardavan, M. Kurmoo, and P. Day, J. Phys.: Condens. Matter **12**, L641 (2000).
[9] S. Manalo and U. Klein, J. Phys.: Condens. Matter **12**, L471 (2000).
[10] S. Uji, H. Shinagawa, T. Terashima, T. Yakabe, Y. Teral, M. Tokumoto, A. Kobayashi, H. Tanaka, and H. Kobayashi, Nature (London) **410**, 908 (2001).
[11] L. Balicas, J. S. Brooks, K. Storr, S. Uji, M. Tokumoto, H. Tanaka, H. Kobayashi, A. Kobayashi, V. Barzykin, and L. P. Gor'kov, Phys. Rev. Lett. **87**, 067002 (2001).
[12] M. Houzet, A. Buzdin, L. Bulaevskii, and M. Maley, Phys. Rev. Lett. **88**, 227001 (2002).
[13] S. Uji, H. Shinagawa, C. Terakura, T. Terashima, T. Yakabe, Y. Terai, M. Tokumoto, A. Kobayashi, H. Tanaka, and H. Kobayashi, Phys. Rev. B **64**, 024531 (2001).
[14] A. Bianchi, R. Movshovich, C. Capan, P. G. Pagliuso, and J. L. Sarrao, Phys. Rev. Lett. **91**, 187004 (2003).
[15] H. Won, K. Maki, S. Haas, N. Oeschler, F. Weickert, and P. Gegenwart, Phys. Rev. B **69**, 180504(R) (2004).
[16] H. A. Radovan, R. J. Zieve, J. S. Kim, and G. R. Stewart, J. Supercond. **16**, 957 (2003).
[17] V. G. Kogan, P. Miranović, Lj. Dobrosavljević-Grujic, W. E. Pickett, and D. K. Christen, Phys. Rev. Lett. **79**, 741 (1997).
[18] R. S. Gonnelli, D. Daghero, A. Calzolari, G. A. Ummarino, V. Dellarocca, V. A. Stepanov, J. Jun, S. M. Kazakov, and J. Karpinski, Phys. Rev. B **69**, 100504(R) (2004).
[19] K. G. Sandeman, G. G. Lonzarich, and A. J. Schofield, Phys. Rev. Lett. **90**, 167005 (2003).
[20] I. I. Mazin, D. J. Singh, and A. Aguayo, in *Proceedings of the NATO Advanced Research Workshop on Physics of Spin in Solids: Materials, Methods, and Applications*, edited by S. Halilov (Kluwer Academic, Boston, 2004); cond-mat/0401563 (unpublished).
[21] E. A. Yelland, S. M. Hayden, S. J. C. Yates, C. Pfleiderer, M. Uhlarz, R. Vollmer, H. von Lohneysen, N. R. Bernhoeft, R. P. Smith, S. S. Saxena, and K. Kimura, cond-mat/0502341 (unpublished).
[22] M. Uhlarz, C. Pfleiderer, and S. M. Hayden, Phys. Rev. Lett. **93**, 256404 (2004).
[23] C. Pfleiderer, M. Uhlarz, S. M. Hayden, R. Vollmer, H. V. Lohneysen, N. R. Bernhoeft, and G. G. Lonzarch, Nature (London) **412**, 58 (2001).
[24] B. J. Powell, J. F. Annett, and B. L. Gyorffy, J. Phys. A **36**, 9289 (2003).
[25] K. Koepernik and H. Eschrig, Phys. Rev. B **59**, 1743 (1999).
[26] D. J. Singh and I. I. Mazin, Phys. Rev. Lett. **88**, 187004 (2002).
[27] A. B. Shick and W. E. Pickett, Phys. Rev. Lett. **86**, 300 (2001).
[28] A. B. Shick, Phys. Rev. B **65**, 180509(R) (2002).
[29] B. T. Matthias, A. M. Clogston, H. J. Williams, E. Corenzwit, and R. C. Sherwood, Phys. Rev. Lett. **7**, 7 (1961).
[30] F. Acker, Z. Fisk, J. L. Smith, and C. Y. Huang, J. Magn. Magn. Mater. **22**, 250 (1981).
[31] T. Sakakibara, T. Tayama, A. Harita, Y. Haga, H. Shishido, R. Settai, and Y. Onuki, Acta Phys. Pol. B **34**, 467 (2003).